# Facile electrochemical synthesis of CeO2 hierarchical nanorods and nanowires with excellent photocatalytic activities

**ARTICLE** *in* NEW JOURNAL OF CHEMISTRY · MAY 2014

Impact Factor: 3.09 · DOI: 10.1039/C4NJ00214H

NJC

PAPER

# Facile electrochemical synthesis of $CeO_2$ hierarchical nanorods and nanowires with excellent photocatalytic activities

Cite this: *New J. Chem.*, 2014, **38**, 2581

Chao Zhang,[a] Xiyue Zhang,[a] Yichen Wang,[a] Shilei Xie,[a] Yi Liu,[b] Xihong Lu*[a] and Yexiang Tong[a]

Received (in Montpellier, France) 11th February 2014,
Accepted 14th March 2014

DOI: 10.1039/c4nj00214h

www.rsc.org/njc

In this work, we developed a simple, cost-effective and controllable electrochemical method to synthesize free-standing $CeO_2$ hierarchical nanorods and nanowires. Due to their hierarchical one-dimensional nanostructures and increased surface areas, both the $CeO_2$ hierarchical nanorods and nanowires exhibit substantially higher photocatalytic performance than the commercial $CeO_2$ nanoparticles in the degradation of methyl orange.

## Introduction

Rare earth oxides, one of the most important families of rare-earth materials, are a particularly interesting class of materials because of their unique optical, electronic, magnetic, and catalytic properties arising from the confinement of the 4f electrons.[1] These unique properties are crucial for many practical applications, such as optical communication, optical displays, efficient catalysis, UV shielding, and medical diagnostics.[2–6] As one of the most functional rare earth oxides, $CeO_2$ has attracted enormous attention due to its excellent physical and chemical properties and wide range of applications in catalysts, fuel cells, UV blockers, solar cells, oxygen storage capacitors and sensors.[7–11] It is widely known that the photocatalytic, magnetic, electronic, and catalytic properties of $CeO_2$ are strongly size/shape dependent at the nanometer scale.[9,12,13] In this regard, considerable effort has been made to design and synthesize $CeO_2$ nanomaterials with controllable morphology and large surface area.[14–19] Among various nanostructures, one-dimensional (1D) $CeO_2$ nanostructures, such as nanorods, nanotubes, and nanowires, have stimulated intensive interest because of their unique optical, electronic, and mechanical properties and potential applications in the fabrication of nanoscale devices.[12,20–23] On the other hand, the assembly of 1D nanostructures into appropriate hierarchical/super-structures has become the focus of research in recent years because they exhibit superior properties compared to the pristine 1D nanostructure.[24–27] For instance, compared with randomly dispersed nanorods, the highly ordered nanorod superstructures can allow for the formation of heterostructures, have larger surface areas, and can form continuous networks.[28] Therefore, once the nanorods as building blocks can be rationally assembled into appropriate three-dimensional (3D) superstructures, they will offer new scientific opportunities for investigating the influence of size and dimensionality with respect to their collective optical, magnetic, and electronic properties.[24,29] Up to now, some $CeO_2$ hierarchical nanostructures such as hierarchical nanospheres,[30,31] nanoflowers[32–34] and urchin-like structures[35] have been reported. Despite these achievements, a simple and efficient method for synthesizing shape-controlled $CeO_2$ 1D hierarchical nanostructures is still lacking.

The electrochemical deposition technique has been widely recognized as a promising alternative candidate for the preparation of nanomaterials because of its low cost, rapidness, environmentally friendly nature and potential advantage of large-scale production.[36–38] Moreover, the operational conditions (applied current or potential and the composition of the electrolyte) usually allow us to modify and control the deposit morphology through changes in mass transport and (electro-)crystallization phenomena.[37,39–41] In recent years, the electrochemical deposition technique has also been employed to synthesize $CeO_2$ nanostructures, and multifarious $CeO_2$ nanostructures including nanospheres,[31] nanorods,[12] nanowires,[42] nanotubes,[43,44] and nanobelts[45] have been successfully synthesized by the electrochemical deposition technique. Nevertheless, to the best of our knowledge, there are few reports on the preparation of $CeO_2$ hierarchical nanostructures *via* the electrochemical deposition technique so far.[17,19,32] In this work, we developed a facile and cost-effective electrochemical deposition method to prepare $CeO_2$ hierarchical nanorods (HNRs) and hierarchical nanowires

[a] *MOE of the Key Laboratory of Bioinorganic and Synthetic Chemistry, KLGHEI of Environment and Energy Chemistry, School of Chemistry and Chemical Engineering, Institute of Optoelectronic and Functional Composite Materials, Sun Yat-Sen University, Guangzhou 510275, China. E-mail: luxh6@mail.sysu.edu.cn*

[b] *School of Chemistry and Chemical Engineering, GuangDong Pharmaceutical University, Guangzhou 510006, China*

(HNWs) and demonstrated their implementation as highly efficient photocatalysts for methyl orange (MO) degradation. This present electrochemical method allows us to easily manipulate the morphology and structure of the product, and free-standing $CeO_2$ HNRs and HNWs could be readily grown on Cu substrates by this electrochemical method. Moreover, both $CeO_2$ HNRs and HNWs exhibit substantially higher photocatalytic performance than the commercial $CeO_2$ nanoparticles (NPs) in the degradation of methyl orange (MO).

## Experimental

### Preparation of $CeO_2$ hierarchical nanorods (HNRs) and nanowires (HNWs)

All reagents used in this work were of analytical grade and were used directly without any purification. All the electrochemical deposition experiments were carried out in a conventional three-electrode glass cell by galvanostatic electrolysis. The working electrode is a Cu foil of 1.5 cm × 3 cm, while the counter electrode and the reference electrode is a graphite rod of about 4.0 $cm^2$ and a saturated Ag/AgCl electrode, respectively. Before electrodeposition, the Cu foil was cleaned ultrasonically in distilled water, ethanol, and acetone and then rinsed in distilled water again. Electrodeposition of $CeO_2$ HNRs was performed in a solution of 0.01 M $Ce(NO_3)_3$ + 0.1 M $NH_4Cl$ + 0.05 M KCl at a current density of 0.44 mA $cm^{-2}$ for 2 h at 70 °C, while that of HNWs was carried out in the same electrolyte at a current density of 0.88 mA $cm^{-2}$ for 2 h at 70 °C.

### Structural and componential characterization

The morphology and structure of products were characterized by scanning electron microscopy (SEM, Quanta 400), X-ray diffraction (XRD, Bruker, D8 ADVANCE) and transmission electron microscopy (TEM, JEM2010-HR). The composition and surface oxidation states of products were studied by X-ray Photoelectron Spectroscopy (XPS, ESCALab250) with 200 W Al KR radiation in a twin anode. The optical properties of the products were measured using a UV-Vis-NIR Spectrophotometer (UV, Shimadzu UV-3150). The BET surface area of samples was characterized by nitrogen adsorption–desorption isotherms at 77 K conducted on an ASAP 2020 V3.03 H instrument. All the samples (powders) were outgassed at 100 °C for 300 min under flowing nitrogen before measurements. For obtaining the SEM, XRD and UV-spectra of $CeO_2$ samples, measurements were directly carried out on the samples without removing the Cu substrates. For the measurements of the TEM, BET surface area and photocatalytic degradation of methyl orange (MO), $CeO_2$ films were exfoliated and ground into powders, which are then used for these tests.

### Photocatalytic tests

Photocatalytic properties of the $CeO_2$ HNRs and HNWs were evaluated using methyl orange (MO) as a demonstration dye under Xe lamp (500 W, Beijing Changtuo, PLSLAX500, wavelength: 200–800 nm) irradiation at room temperature with cooling water. Typically, 20 mg of $CeO_2$ samples (powders) was suspended in 100 ml of 20 mg $L^{-1}$ MO aqueous solution (pH = 3). The suspension was magnetically stirred in the dark for 24 h to ensure establishment of an adsorption–desorption equilibrium before light irradiation. Then, at different light irradiation intervals, 3 ml of the suspensions was collected, filtered through a 0.45 lm membrane, and finally analyzed using a Shimadzu UV-3150a UV-Vis-NIR spectrophotometer immediately.

## Results and discussion

Electrodeposition of $CeO_2$ HNRs was performed in a solution of 0.01 M $Ce(NO_3)_3$ + 0.1 M $NH_4Cl$ + 0.05 M KCl at a current density of 0.44 mA $cm^{-2}$ for 2 h at 70 °C. Fig. 1 displays the typical scanning electron microscopy (SEM) images of the $CeO_2$ HNRs. It can be clearly observed that $CeO_2$ flower-like nanostructures consisting of high density nanorods were successfully grown on Cu substrates. These $CeO_2$ nanorods are uniform and have a diameter of around 200–250 nm. More interestingly, the $CeO_2$ nanorods were constructed using a large number of $CeO_2$ nanowires with a small size (Fig. 1c). To identify the crystalline phase of the product, the X-ray diffraction (XRD) spectrum of $CeO_2$ HNRs was collected and is shown in Fig. 1d. Besides the Cu peaks coming from the Cu substrates, all of the peaks in the XRD spectrum can be well indexed to a fluorite cubic structure of $CeO_2$ (JCPDF # 65-2975) with lattice constant $a$ = 0.5411 nm. No other peaks were detected, indicating that the product is highly pure. Additionally, the relatively strong intensity of $CeO_2$ peaks suggests that the $CeO_2$ HNRs possess good crystallinity.

To investigate the microstructure of $CeO_2$ HNRs, transmission electron microscopy (TEM) analysis was performed. Fig. 2a shows a typical TEM image of a single $CeO_2$ HNR, whose diameter is about 200 nm, which is in accordance with the

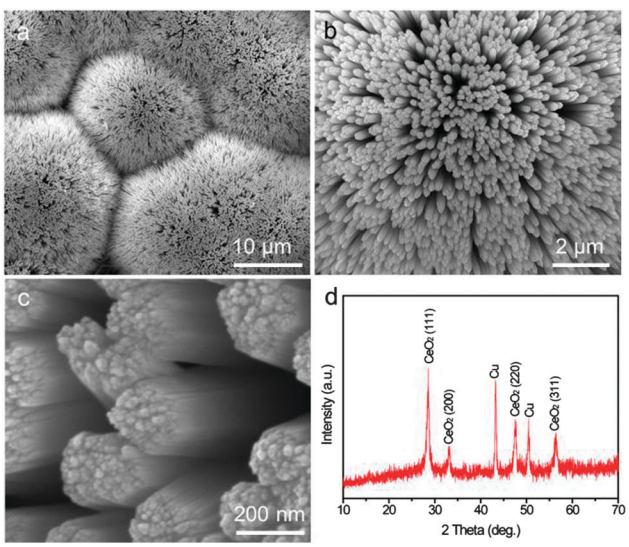


Fig. 1 (a–c) SEM images and (d) the XRD spectrum of $CeO_2$ HNRs prepared with a current density of 0.44 mA $cm^{-2}$.

 

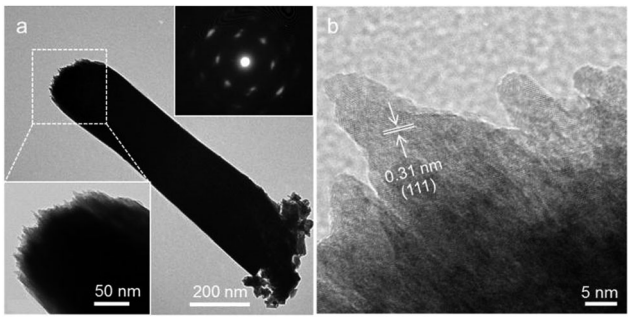


Fig. 2 (a) TEM image and (b) HRTEM image of the $CeO_2$ nanorods. The insets are the enlarged TEM image and corresponding SAED pattern.

SEM results. The enlarged TEM image (inset in Fig. 2a) reveals that this $CeO_2$ nanorod is made up of numerous nanowires. The corresponding selected area electron diffraction (SAED) pattern of this $CeO_2$ nanorod is shown in Fig. 2a. The bright diffraction spots confirm the highly crystalline nature of this nanorod, and more evidence can be obtained from the HRTEM observation.[15] Fig. 2b presents the high-resolution TEM (HRTEM) image of the $CeO_2$ nanorod. The well-resolved two-dimensional lattice fringes again confirm that the $CeO_2$ nanorod has a high crystallinity.[15,18] The lattice fringe with a *d*-spacing of 0.31 nm matches well with the (111) interplanar spacing of face-centered-cubic $CeO_2$.

X-ray photoelectron spectroscopy (XPS) analysis was also conducted to further study the composition of $CeO_2$ HNRs. The XPS survey spectrum of $CeO_2$ HNRs is presented in Fig. 3a. Only Ce, C and O signals are observed on the surface of the sample, which indicates the high purity of the $CeO_2$ HNRs because the C signal originates from the adventitious carbon. Fig. 3b displays the Ce 3d core level XPS spectrum of $CeO_2$ HNRs, which can be deconvolved into eight peaks. The peaks labeled as $v_1$ and $u_1$ are the characteristic peaks of $Ce^{3+}$ states while others are the characteristic peaks of $Ce^{4+}$ states.[46] This result indicates that $Ce^{4+}$ ions are dominant in the deposit and a small quantity of $Ce^{3+}$ is also present in this deposit. Fig. 3c shows the O 1s core level XPS spectrum of $CeO_2$ HNRs, which can be deconvolved into two peaks. The peak centered at 529.4 eV is assigned to the oxygen bond of Ce–O–Ce, and the peak located at 531.3 eV corresponds to Ce–O–H, respectively.[47] The XPS results mentioned above reveal that the as-deposited product is mainly $CeO_2$, which is consistent with the XRD and TEM analyses.[20,45]

Our present electrochemical method allows further structural manipulation. As shown in Fig. 4a, a new kind of $CeO_2$ spear-like hierarchical nanowires (denoted as HNWs) was successfully obtained when the deposition current density was simply increased to 0.88 mA $cm^{-2}$. The enlarged SEM images show that these $CeO_2$ HNWs with a diameter of about 100 nm vertically grew on Cu substrates (Fig. 4b and the inset). A typical TEM image of a single $CeO_2$ HNW is shown in Fig. 4c. The spear-like morphology of the HNW is distinctly observed, and the diameter of this HNW (measured in middle) is about 80 nm. Fig. 4d shows the enlarged TEM image taken from the red rectangle part of the HNW (Fig. 4c), showing that this

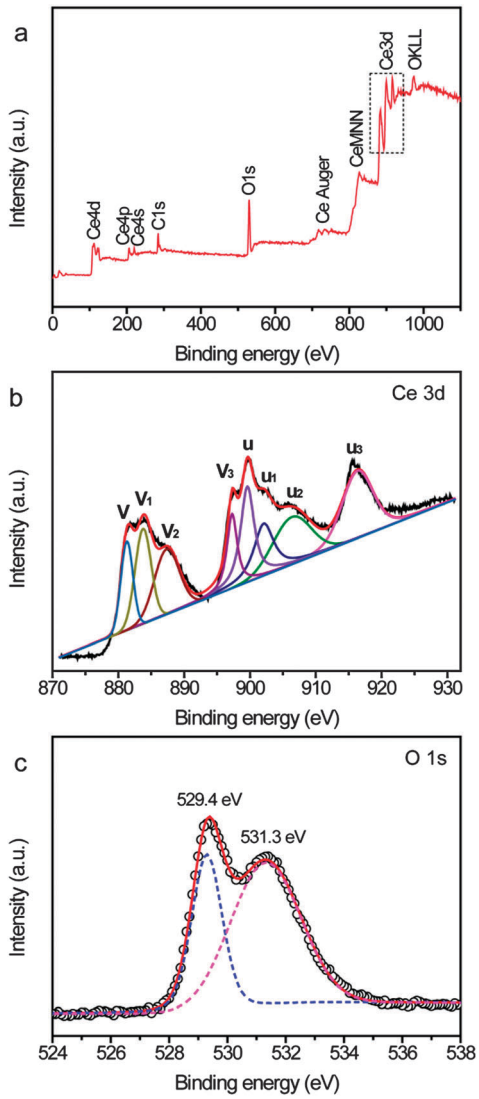


Fig. 3 (a) XPS survey spectrum, (b) Ce 3d core level XPS spectrum and (c) O 1s core level XPS spectrum of the as-prepared $CeO_2$ HNRs.

HNW is composed of several small size nanowires (indicated by red arrows). Fig. 4e displays the HRTEM image of the $CeO_2$ HNW taken from the red circle part. The well-resolved lattice fringes clearly demonstrate that the $CeO_2$ HNW also has a high degree of crystallinity. The lattice fringe with the spacing of 0.31 nm corresponds to the (111) interplanar spacing of cubic $CeO_2$. Additionally, SAED analysis confirms that the $CeO_2$ HNW is highly crystalline (inset in Fig. 4e).

Fig. 5a shows the nitrogen adsorption–desorption isotherms of the $CeO_2$ HNRs and HNWs collected at 77 K. Both the $CeO_2$ HNRs and HNWs exhibited typical Langmuir IV characteristics with an obvious hysteresis loop, suggesting that there are mesopores in $CeO_2$ HNRs and HNWs. The specific surface areas of $CeO_2$ HNRs and HNWs calculated by the Brunauer–Emmett–Teller (BET) method are 58.6 and 69.4 $m^2\ g^{-1}$, respectively. Fig. 5b shows the UV-visible absorption spectra of the $CeO_2$ HNRs and HNWs. Both the samples exhibited a similar absorption band edge at about 390 nm, which is consistent

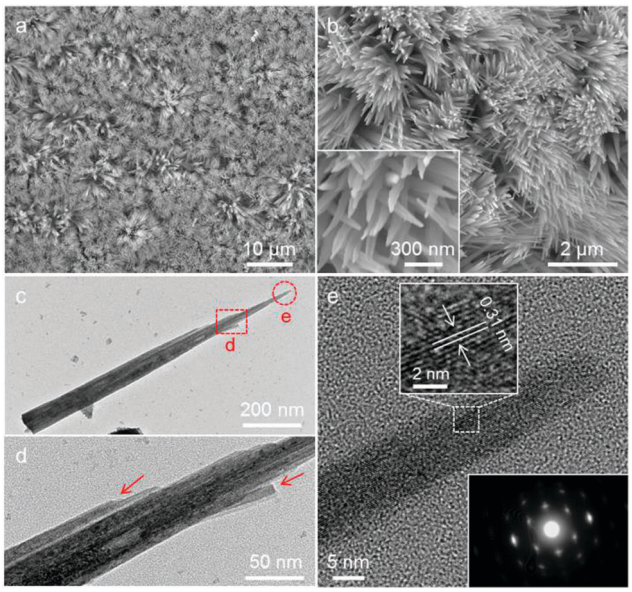


Fig. 4 (a and b) SEM images, (c and d) TEM images and (e) HRTEM image of $CeO_2$ HNWs prepared with a current density of 0.88 mA $cm^{-2}$. The insets in Fig. 4e show the enlarged HRTEM image and the corresponding SAED pattern.

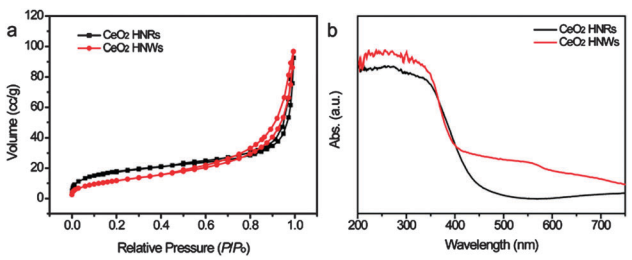


Fig. 5 (a) Nitrogen adsorption–desorption isotherms of the $CeO_2$ HNRs and HNWs at 77 K.

with the $CeO_2$ band-gap of 3.2 eV.[7,12] In comparison to the $CeO_2$ HNRs, the $CeO_2$ HNWs display higher absorption in the wavelength range between 400 and 750 nm, suggesting that the $CeO_2$ HNWs could utilize visible light.

To study the photocatalytic activities of the as-prepared $CeO_2$ samples, their efficiencies for the photocatalytic degradation of MO under light irradiation were measured. For better comparison, commercial $CeO_2$ nanoparticles (NPs) and $TiO_2$ nanoparticles (P25, Degussa) were also examined in the same test. Before the photocatalytic tests, the $CeO_2$ samples were magnetically stirred in the dark for 12 h to establish the adsorption–desorption equilibrium. Fig. 6 compares the efficiencies of different samples for the photodegradation of MO as a function of irradiation time. The *y*-axis is defined as $C_t/C_0$, where $C_t$ is the main absorption peak intensity of MO sampled at each irradiated time interval and $C_0$ is the absorption intensity of the starting concentration. Significantly, both the $CeO_2$ HNRs and HNWs exhibited a substantially faster degradation rate of MO than the commercial $CeO_2$ NPs and P25. After 180 min light irradiation, the photocatalytic degradation

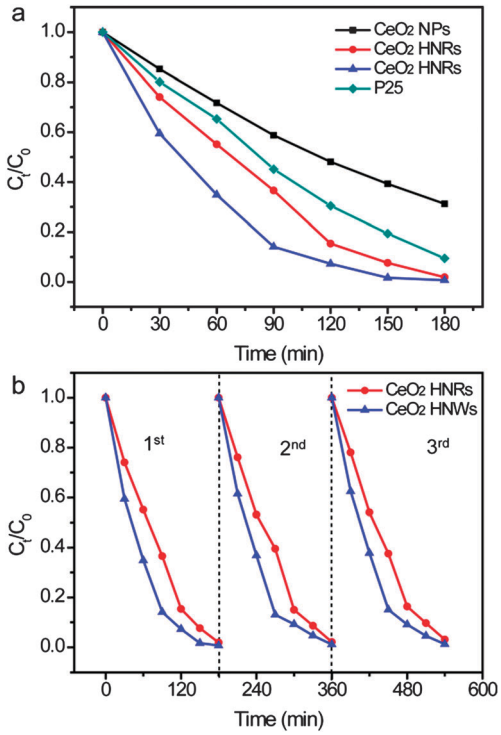


Fig. 6 (a) Photodegradation efficiencies of commercial $CeO_2$ NPs, P25, $CeO_2$ HNRs and $CeO_2$ HNWs for MO as a function of light irradiation time. (b) Cycling performance of $CeO_2$ HNRs and $CeO_2$ HNWs for MO degradation.

efficiencies of MO solution for $CeO_2$ HNRs and HNWs reached 98.2% and 99.3%, while those of the commercial $CeO_2$ NPs and P25 were only 68.8% and 89.5% respectively. Moreover, the $CeO_2$ HNRs and HNWs have good cycling stability. As shown in Fig. 6b, both the $CeO_2$ HNRs and HNWs exhibited no any decay of their photocatalytic activities after three cycles. The BET surface area of $CeO_2$ HNRs (58.6 $m^2$ $g^{-1}$) and HNWs (69.4 $m^2$ $g^{-1}$) is higher than the commercial $CeO_2$ NPs (50.2 $m^2$ $g^{-1}$). Additionally, these hierarchical 1D nanorods and nanowires not only can provide large interface areas for photocatalytic reaction, but also shorten the diffusion pathway for minority carriers.[48–50] Therefore, such superior photocatalytic performances of $CeO_2$ HNRs and HNWs are mainly attributed to their hierarchical 1D nanostructures and higher surface areas. On the other hand, compared to the $CeO_2$ HNRs, the $CeO_2$ HNWs show a faster degradation rate of MO. As indicated in Fig. 5b, the $CeO_2$ HNWs have stronger absorption than the $CeO_2$ HNRs in the visible light region, and hence the $CeO_2$ HNWs may absorb more light and generate more electrons and holes than the $CeO_2$ HNRs at the same time. The superior photoactivity of $CeO_2$ HNWs compared to the HNRs is due to their larger surface area and improved light-harvesting ability.

## Conclusions

In summary, free-standing $CeO_2$ HNRs and HNWs were successfully synthesized on Cu substrates by a simple, low cost and

 

environmentally friendly electrochemical deposition approach. The morphology and structure of the products can be readily controlled by simply adjusting the current density. Furthermore, both the $CeO_2$ HNRs and HNWs could remove 98.2% and 99.3% of MO under light irradiation for 180 min, which is substantially higher than the commercial $CeO_2$ NPs (68.8%) and P25 (89.5%). The superior photocatalytic performance can be attributed to their increased surface areas and hierarchical 1D nanostructures that provide more active sites for photocatalytic reaction and a shorter diffusion length for minority carriers. This work not only demonstrates a facile electrochemical method to synthesize $CeO_2$ hierarchical 1D nanostructures, but may also open up new opportunities for the design and preparation of highly efficient photocatalysts.

## Acknowledgements

We acknowledge the financial support from the Natural Science Foundations of China (21273290, 91323101 and J1103305), the Research Fund for the Doctoral Program of Higher Education of China (20120171110043), the Young Teacher Starting-up Research program of Sun Yat-Sen University and the Laboratory opening Fund of Sun Yat-sen University.

## Notes and references

1 Z.-G. Yan and C.-H. Yan, *J. Mater. Chem.*, 2008, **18**, 5046–5059.
2 G.-y. Adachi and N. Imanaka, *Chem. Rev.*, 1998, **98**, 1479–1514.
3 R. Li, S. Yabe, M. Yamashita, S. Momose, S. Yoshida, S. Yin and T. Sato, *Mater. Chem. Phys.*, 2002, **75**, 39–44.
4 R. Li, S. Yabe, M. Yamashita, S. Momose, S. Yoshida, S. Yin and T. Sato, *Solid State Ionics*, 2002, **151**, 235–241.
5 M. V. Ganduglia-Pirovano, A. Hofmann and J. Sauer, *Surf. Sci. Rep.*, 2007, **62**, 219–270.
6 S. Yin, Y. Minamidate, S. Tonouchi, T. Goto, Q. Dong, H. Yamane and T. Sato, *RSC Adv.*, 2012, **2**, 5976–5982.
7 X. Lu, T. Zhai, H. Cui, J. Shi, S. Xie, Y. Huang, C. Liang and Y. Tong, *J. Mater. Chem.*, 2011, **21**, 5569–5572.
8 C. W. Sun, H. Li and L. Q. Chen, *Energy Environ. Sci.*, 2012, **5**, 8475–8505.
9 D. Zhang, X. Du, L. Shi and R. Gao, *Dalton Trans.*, 2012, **41**, 14455–14475.
10 H. Yu, Y. Bai, X. Zong, F. Tang, G. M. Lu and L. Wang, *Chem. Commun.*, 2012, **48**, 7386–7388.
11 X. Zhao, Y. Du, W. Ye, D. Lu, X. Xia and C. Wang, *New J. Chem.*, 2013, **37**, 4045–4051.
12 X. H. Lu, D. Z. Zheng, P. Zhang, C. L. Liang, P. Liu and Y. X. Tong, *Chem. Commun.*, 2010, **46**, 7721–7723.
13 J. Zhang, H. Kumagai, K. Yamamura, S. Ohara, S. Takami, A. Morikawa, H. Shinjoh, K. Kaneko, T. Adschiri and A. Suda, *Nano Lett.*, 2011, **11**, 361–364.
14 L. González-Rovira, J. M. Sánchez-Amaya, M. López-Haro, E. Del Rio, A. B. Hungría, P. Midgley, J. J. Calvino, S. n. Bernal and F. J. Botana, *Nano Lett.*, 2009, **9**, 1395–1400.
15 X. H. Lu, X. Huang, S. L. Xie, D. Z. Zheng, Z. Q. Liu, C. L. Liang and Y. X. Tong, *Langmuir*, 2010, **26**, 7569–7573.
16 Q. Yuan, H. H. Duan, L. L. Li, Z. X. Li, W. T. Duan, L. S. Zhang, W. G. Song and C. H. Yan, *Adv. Mater.*, 2010, **22**, 1475–1478.
17 Y. Zheng, K. Liu, H. Qiao, Y. Zhang, Y. Song, M. Yang, Y. Huang, N. Guo, Y. Jia and H. You, *CrystEngComm*, 2011, **13**, 1786–1788.
18 Z. Ji, X. Wang, H. Zhang, S. Lin, H. Meng, B. Sun, S. George, T. Xia, A. E. Nel and J. I. Zink, *ACS Nano*, 2012, **6**, 5366–5380.
19 F. Meng, F. Lu, L. Wang, J. Cui and J. Lu, *Sci. Adv. Mater.*, 2012, **4**, 1018–1023.
20 G. R. Li, D. L. Qu, L. Arurault and Y. X. Tong, *J. Phys. Chem. C*, 2009, **113**, 1235–1241.
21 Z.-R. Tang, Y. Zhang and Y.-J. Xu, *RSC Adv.*, 2011, **1**, 1772–1777.
22 P. Pal, S. K. Pahari, A. Sinhamahapatra, M. Jayachandran, G. M. Kiruthika, H. C. Bajaj and A. B. Panda, *RSC Adv.*, 2013, **3**, 10837–10847.
23 R. Pérez-Hernández, G. Mondragon-Galicia, A. Allende and J. Palacios, *Phys. Chem. Chem. Phys.*, 2013, **15**, 12702–12708.
24 J. N. Tiwari, R. N. Tiwari and K. S. Kim, *Prog. Mater. Sci.*, 2012, **57**, 724–803.
25 C. Z. Yao, B. H. Wei, H. X. Ma, H. Li, L. X. Meng, X. S. Zhang and Q. J. Gong, *J. Power Sources*, 2013, **237**, 295–299.
26 B. Liu, P. Soares, C. Checkles, Y. Zhao and G. Yu, *Nano Lett.*, 2013, **13**, 3414–3419.
27 X. Luo, Z. Lou, L. Wang, X. Zheng and T. Zhang, *New J. Chem.*, 2014, **38**, 84–89.
28 S. Xie, X. Lu, T. Zhai, J. Gan, W. Li, M. Xu, M. Yu, Y.-M. Zhang and Y. Tong, *Langmuir*, 2012, **28**, 10558–10564.
29 L. S. Zhong, J. S. Hu, H. P. Liang, A. M. Cao, W. G. Song and L. J. Wan, *Adv. Mater.*, 2006, **18**, 6.
30 H. Y. Xiao, Z. H. Ai and L. Z. Zhang, *J. Phys. Chem. C*, 2009, **113**, 16625–16630.
31 X. W. Ouyang, W. Li, S. L. Xie, T. Zhai, M. H. Yu, J. Y. Gan and X. H. Lu, *New J. Chem.*, 2013, **37**, 585–588.
32 R. Yu, L. Yan, P. Zheng, J. Chen and X. Xing, *J. Phys. Chem. C*, 2008, **112**, 19896–19900.
33 J. J. Wei, Z. J. Yang, H. X. Yang, T. Sun and Y. Z. Yang, *CrystEngComm*, 2011, **13**, 4950–4955.
34 N. S. Arul, D. Mangalaraj and T. W. Kim, *Appl. Phys. Lett.*, 2013, **102**, 223115.
35 J. Wei, Z. Yang and Y. Yang, *CrystEngComm*, 2011, **13**, 2418–2424.
36 X. Lu, D. Zheng, T. Zhai, Z. Liu, Y. Huang, S. Xie and Y. Tong, *Energy Environ. Sci.*, 2011, **4**, 2915–2921.
37 G.-R. Li, H. Xu, X.-F. Lu, J.-X. Feng, Y.-X. Tong and C.-Y. Su, *Nanoscale*, 2013, **5**, 4056–4069.
38 H. Li, C. Yao, L. Meng, H. Sun, J. Huang and Q. Gong, *Electrochim. Acta*, 2013, **108**, 45–50.
39 Y. T. Kim, J. H. Han, B. H. Hong and Y. U. Kwon, *Adv. Mater.*, 2010, **22**, 515–518.

40 X. Lu, X. Huang, S. Xie, T. Zhai, C. Wang, P. Zhang, M. Yu, W. Li, C. Liang and Y. Tong, *J. Mater. Chem.*, 2012, **22**, 13357–13364.
41 H. Li, C. Chen, X. Huang, Y. Leng, M. Hou, X. Xiao, J. Bao, J. You, W. Zhang, Y. Wang, J. Song, Y. Wang, Q. Liu and G. A. Hope, *J. Power Sources*, 2014, **247**, 915–919.
42 X. H. Lu, D. Z. Zheng, J. Y. Gan, Z. Q. Liu, C. L. Liang, P. Liu and Y. X. Tong, *J. Mater. Chem.*, 2010, **20**, 7118–7122.
43 M. Xu, S. L. Xie, X. H. Lu, Z. Q. Liu, Y. Y. Huang, Y. F. Zhao, J. Q. Ye and Y. X. Tong, *J. Electrochem. Soc.*, 2011, **158**, E41–E44.
44 C.-h. Zeng, S. Xie, M. Yu, Y. Yang, X. Lu and Y. Tong, *J. Power Sources*, 2014, **247**, 545–550.
45 G.-R. Li, D.-L. Qu and Y.-X. Tong, *Electrochem. Commun.*, 2008, **10**, 80–84.
46 P. Burroughs, A. Hamnett, A. F. Orchard and G. Thornton, *J. Chem. Soc., Dalton Trans.*, 1976, 1686–1698.
47 H.-I. Chen and H.-Y. Chang, *Solid State Commun.*, 2005, **133**, 593–598.
48 I. Gonzalez-Valls and M. Lira-Cantu, *Energy Environ. Sci.*, 2009, **2**, 19–34.
49 K. Nakata and A. Fujishima, *J. Photochem. Photobiol., C*, 2012, **13**, 169–189.
50 Y. Wang, Q. Wang, X. Zhan, F. Wang, M. Safdar and J. He, *Nanoscale*, 2013, **5**, 8326–8339.

 